Journal of Molecular Structure 1183 (2019) 126–136

Contents lists available at ScienceDirect

Journal of Molecular Structure

journal homepage: http://www.elsevier.com/locate/molstruc

The impact of dextran sulfate on the radiolytic synthesis of magnetic iron oxide nanoparticles

Ivan Marić [a], Goran Štefanić [b, c], Marijan Gotić [b, c, *], Tanja Jurkin [a, *]

[a] Radiation Chemistry and Dosimetry Laboratory, Division of Materials Chemistry, Ruđer Bošković Institute, Bijenička 54, 10 000, Zagreb, Croatia
[b] Laboratory for Molecular Physics and Synthesis of New Materials, Division of Materials Physics, Ruđer Bošković Institute, Bijenička 54, 10 000, Zagreb, Croatia
[c] Center of Excellence for Advanced Materials and Sensing Devices, Research Unit New Functional Materials, Ruđer Bošković Institute, Bijenička 54, 10 000, Zagreb, Croatia

ARTICLE INFO

Article history:
Received 24 September 2018
Received in revised form
2 January 2019
Accepted 24 January 2019
Available online 25 January 2019

Keywords:
Gamma-irradiation
Dextran sulfate
Green rust
Iron(II) hydroxide
Feroxyhyte
Mackinawite

ABSTRACT

Iron(III) chloride deoxygenated alkaline aqueous colloidal solutions in the presence of 2-propanol and dextran sulfate were γ-irradiated with doses of 36 and 130 kGy. The dose rate was ~31 kGy h^{-1}. The samples isolated by washing with water mainly consisted of γ-FeOOH (lepidocrocite), δ-FeOOH and schwertmannite. The samples isolated by washing with ethanol contained mainly α-FeOOH (goethite), δ-FeOOH (feroxyhyte) and iron(III) hydroxide sulfate. At lower dose (36 kGy) magnetite (Fe_3O_4) was formed. The samples isolated by admixing glycerol consisted of the intermediate phases $Fe(OH)_2$, $GR(SO_4^{2-})$ and non-stoichiometric FeS_{1-x} (mineral name mackinawite). The amounts of Fe(II) in glycerol-isolated solid samples were 60.5% and 82.6% as determined by Mössbauer spectroscopy at doses of 36 and 130 kGy, respectively. The amount of Fe^{2+} in the acidified solutions containing dissolved γ-irradiation products was determined using potassium permanganate titration. The amounts of Fe^{2+} in acidified solutions were 72.0% and 92.0% at doses of 36 and 130 kGy, respectively. Thus, although the conventionally isolated powders consisted exclusively of Fe(III) products, the high reducing conditions upon γ-irradiation were confirmed by capturing the Fe(II) intermediate phases and by quantitative determinations of ferrous ions in the solid samples and solutions containing dissolved γ-irradiation products.

1. Introduction

The synthetic iron oxide chemistry has a long tradition [1–14]. On the contrary, the γ-irradiation (radiolytical) synthesis of iron oxide nanoparticles (NPs) has been less intensively investigated [15–21]. The radiolytical synthesis has been predominantly used for the synthesis of magnetite or maghemite NPs. Wang et al. [20,21] have reported the transformation of akaganeite (β-FeOOH) to magnetite in a γ-irradiated aqueous suspension containing 20 vol% of isopropanol as a hydroxyl scavenger. They performed the γ-irradiation experiments under constant stirring. In this way akaganeite particles were mechanically dispersed in an aqueous suspension by stirring, thus enabling a good contact between the solid and liquid phases. Jurkin et al. [17] have shown that ferrihydrite nanoparticles settled at the bottom of a flask did not transform to magnetite (Fe_3O_4) or to any other iron oxide phase upon γ-irradiation in ethanol suspension. Accordingly, to ensure and to maintain the well dispersed system is as important as achieving the reducing conditions upon γ-irradiation. For instance, the well-dispersed ferrihydrite NPs formed in a microemulsion transformed easily to substoichiometric magnetite NPs upon γ-irradiation [16]. Typically, various polymers and surfactants can be used as nanoparticle dispersants, surface stabilizers, growth modifiers and reducing agents [22–24]. Polymers inhibit coalescence and aggregation of metal oxide NPs through steric hindrances or electrostatic repulsion. In addition to inhibiting aggregation and increasing the colloidal stability of NPs, polymers and surfactants can kinetically control the growth of specific facets thus affecting the particle morphology [25].

Generally, the radiolytic synthesis is a powerful method for the synthesis of iron oxide NPs of controlled size, shape and phase

* Corresponding authors. Ruđer Bošković Institute, Bijenička 54, 10000, Zagreb, Croatia.
E-mail addresses: gotic@irb.hr (M. Gotić), tjurkin@irb.hr (T. Jurkin).

https://doi.org/10.1016/j.molstruc.2019.01.075
0022-2860/

composition [16,19–21,26]. It takes an advantage of high-energy γ-radiation (1.25 MeV for ^{60}Co γ-rays) that is able to ionize an aqueous phase. On irradiation of metal oxide precursors dissolved in aqueous solution γ-irradiation generates a variety of species such as free radicals (e^-_{aq}, $H^\bullet$, $^\bullet OH$, $HO^\bullet_2$) and molecular products (H_2, H_2O_2), mainly products of water radiolysis. The main advantage of the γ-irradiation is its high reductive power, i.e. γ-irradiation produces a mass of reductive radicals (mostly e^-_{aq} and $H^\bullet$) homogenously through the sample. By adjusting the irradiation dose and dose rate, atmosphere and pH of irradiated suspensions the reducing conditions as well as size, shape and phase composition of formed metal, metal oxide and alloys NPs can be appropriately controlled [15–21,26–30]. However, metal oxides NPs are much difficult to stabilize and protect against oxidation in comparison to noble metal NPs. Stoichiometric magnetite NPs (Fe_3O_4) contains 33% of ferrous ions (Fe^{2+}) that are highly susceptible to the presence of oxygen and can easily oxidize in the aqueous suspensions or atmospheric conditions. The stoichiometry of γ-irradiation synthesized magnetite NPs depends on absorbed dose and dose rate [16]. Du and Liu [31] prepared superparamagnetic γ-Fe_2O_3 NPs in non-aqueous medium by γ-irradiating ferrocene in the presence of isopropyl alcohol. The authors suggested that γ-irradiation produced Fe^0 NPs that then oxidized to γ-Fe_2O_3 in the air during the isolation of precipitates. Ekoko et al. [32] showed that the pH value of Fe(III) solution before the γ-irradiation had influence on the morphology and phase composition of the iron oxides (Fe_3O_4 or α-Fe_2O_3). Yakabuskie et al. [33] prepared uniform-sized γ-FeOOH colloidal nanoparticles by γ-irradiation of deaerated aqueous solutions containing soluble Fe^{2+} species at pH 5.5. At short irradiation times (low dose) spherical particles with a size less than 10 nm were formed, whereas at longer irradiation the final size of the large particles was 60 nm. Sutherland et al. [29] synthesized magnetite NPs by γ-radiolysis of solutions containing different initial concentrations of $FeSO_4$ without any other chemical additives. The authors suggested that the radiolytic cycles of reductive dissolution and oxidative precipitation were responsible for the magnetite NPs formation.

In our previous work [18], we have shown that γ-irradiation of an iron(III) chloride alkaline aqueous solution in the presence of high molecular weight PEO produced rigid hydrogels with embedded iron oxide nanoparticles. γ-irradiation of iron(III) chloride alkaline aqueous solution in the presence of PVP produced a magnetic suspension due to the formation of a small amount of δ-FeOOH (feroxyhyte). On the other hand, γ-irradiation of iron(III) chloride alkaline aqueous solution in the presence of diethylaminoethyl-dextran hydrochloride (DEAE-dextran) produced almost pure δ-FeOOH nanodiscs [19]. The synthesis of δ-FeOOH nanodiscs using γ-irradiation is quite unexpected and we supposed that γ-irradiation reduced Fe(III) and that δ-FeOOH nanodiscs were formed through oxidation of $Fe(OH)_2$ and Green Rust I intermediate products. In this work, instead of DEAE-dextran we used dextran sulfate polymer in a form of sodium salt. The motivation for using dextran sulfate is the presence of sulfate groups that can form Green Rust II (GR SO_4^{2-}) under reducing conditions [34–39]. Dextran sulfate is a biocompatible and biodegradable branched negatively charged polysaccharide of anhydroglucose units. It contains approximately 17% ester bonded sulfur, what is equivalent to approximately 2.3 sulfate groups per glucosyl unit. Dextran sulfates are supplied as the sodium salt form, making them soluble and stable in water. It has been used in pharmaceutical and biomedical field, in drug delivery, for lipoprotein separation, as anticoagulant agent and it has antiviral properties [40–42]. Therefore, in this work we applied γ-irradiation to the Fe(III)/dextran-sulfate/2-propanol alkaline deoxygenated suspensions in order to study the impact of dextran sulfate on the radiolytical synthesis of magnetic iron oxide particles. The highly reactive Fe(II) intermediate phases were isolated by admixing glycerol and thereby confirmed the reducing conditions created by γ-irradiation.

2. Materials and methods

2.1. Chemicals

Iron(III) chloride hexahydrate ($FeCl_3{\cdot}6H_2O$) (puriss. p.a., Reag. Ph. Eur., ≥99%) supplied by *Sigma-Aldrich,* dextran sulfate sodium salt from *Leuconostoc spp*. prepared from dextran of average molecular weight M.W.>500,000 by *Sigma*, sodium hydroxide (p.a.) by *LachNer*, 2-propanol (CHROMASOLV, for HPLC, ≥99.9%) by *Honeywell*, glycerol by *LachNer* (anhydrous, p.a.), absolute ethanol (p.a.) by *J. T. Baker* and Milli-Q deionized water were used.

2.2. Synthesis

0.475 g of $FeCl_3{\cdot}6H_2O$ and 1.85 g of dextran sulfate sodium salt were dissolved in 100 mL of Milli-Q water and then 1.54 mL of 2-propanol was added. The final concentrations of Fe^{3+} and 2-propanol in solution were $1.72\cdot10^{-2}$ and 0.2 mol dm^{-3}, respectively. The final concentration of dextran sulfate was 1.82 wt%. The pHs of thus prepared solutions were adjusted to 9 by adding 2 M NaOH aqueous solution. The precursor suspensions were bubbled with nitrogen through rubber septa for at least 20 min in order to remove the dissolved oxygen. Thus obtained deoxygenated colloidal solutions were γ-irradiated (without stirring) in a septum-closed glass flask. γ-irradiation was performed in a ^{60}Co γ-irradiation facility located in the Radiation Chemistry and Dosimetry Laboratory at the Ruđer Bošković Institute, Zagreb, Croatia. The dose rate of γ-radiation was ~31 kGy h^{-1}. The absorbed doses were 36 and 130 kGy.

Upon the γ-irradiation the reddish colloidal solution turned to black/dark brown or to white-pale blue-green upon the γ-irradiation at 36 or 130 kGy, respectively. The suspensions were isolated in four different ways: *i)* opening the glass flask followed with properly washing/centrifugation with deionized water (samples S-36W, S-130W and S-130W1); *ii)* opening the glass flask followed with properly washing/centrifugation with ethanol (samples S-36E, S-130E and S-130E1); *iii)* by admixing glycerol through septum and then, opening the glass flask followed with a centrifugation (samples S-36G and S-130G); *iv)* opening the glass flask followed with a centrifugation without admixing glycerol or washing (sample S-130U). In all four procedures the isolated precipitates were dried in vacuum at room temperature and analyzed as pastes or powders. Fig. 1 shows the graphical representation of the samples synthesis, isolation and characterization, whereas the annotation of samples and detailed experimental conditions are given in Table 1. It should be pointed out here that we used Roman numerals (e.g., Fe(II) or Fe(III) to denote structural iron ions in solid samples, whereas Arabic numerals (e.g., Fe^{2+} or Fe^{3+}) were used for the dissolved iron ions in clear solutions.

2.3. Characterization of samples

The morphology of the samples was evaluated using a field emission scanning electron microscope (FE SEM, model JSM-7000F) manufactured by *JEOL Ltd.* connected to the EDS/INCA 350 (energy dispersive X-ray analyzer) manufactured by Oxford Instruments.

X-ray powder diffraction (XRD) patterns were recorded at 20 °C using the APD 2000 X-ray powder diffractometer (Cu*Kα* radiation, graphite monochromator, NaI–Tl detector) manufactured by

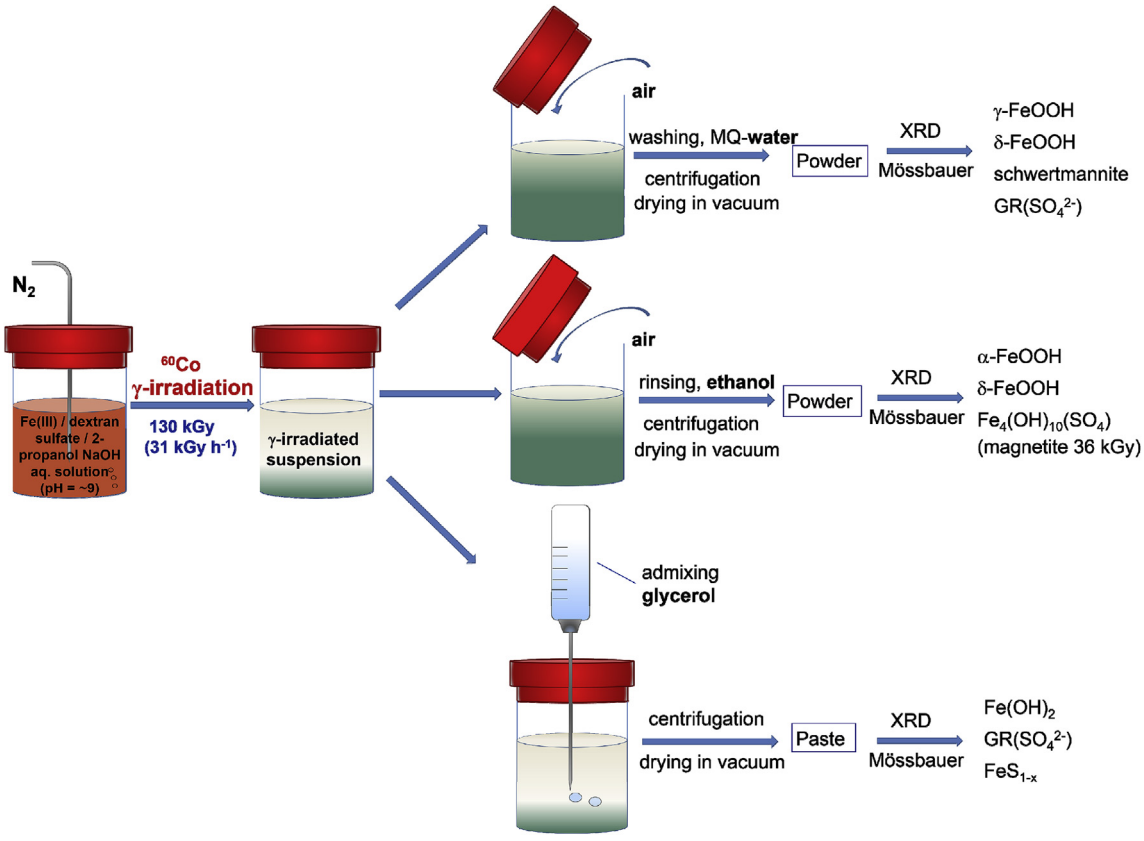

Fig. 1. The graphical representation of the samples synthesis, isolation and characterization.

Table 1
Annotation of samples, γ-irradiation doses, isolation procedure, results of phase analysis, percentage of Fe(II) determined by Mössbauer spectroscopy, percentage of Fe^{2+} in acidified solutions containing dissolved γ-irradiation products and magnetic properties of isolated samples.

Sample	Dose (kGy)	Isolation procedure					Phase analysis* (based on XRD and Mössbauer results)	Fe(II) in solid samples/Fe^{2+} in acidified solutions (%)	Attracted by magnet***
		Unwashed	Admixing glycerol	Washing (water)	Rinsing (ethanol)	Aged 1 day			
S-130W1	130			+		+	γ-FeOOH δ-FeOOH $GR(SO_4^{2-})$	5.7	+
S-130W	130			+			γ-FeOOH δ-FeOOH Schwertmannite		+
S-36W	36			+			γ-FeOOH δ-FeOOH Schwertmannite		+
S-130E1	130				+	+	α-FeOOH δ-FeOOH iron(III) sulfate hydroxide		+
S-130E	130				+		α-FeOOH δ-FeOOH iron(III) sulfate hydroxide		+
S-36E	36				+		$Fe_{3-x}O_4$ (substoichiometric magnetite)		+
S-130G	130		+				$Fe(OH)_2$ $GR(SO_4^{2-})$ FeS_{1-x} (mackinawite)	82.6/92.0**	****
S-36G	36		+				$GR(SO_4^{2-})$	60.5/72.0**	****
S-130U	130	+					$Fe(OH)_2$ $GR(SO_4^{2-})$ δ-FeOOH	7.2	+

*Only those phases that agree with the XRD and Mössbauer assignations are listed.
**The amount of Fe^{2+} in acidified solutions containing dissolved γ-irradiation products as determined by $KMnO_4$ titration. The amounts of Fe^{2+} in the solutions were 92.0% and 72.0%, which are in very good agreement with the Fe(II) values of 82.6% and 60.5% as determined by Mössbauer spectroscopy in the isolated solid samples.
***Magnetic properties of powder samples were checked with a permanent magnet at room temperature.
****The attraction of sample by magnet was not able to test, because the sample was isolated in the form of a paste.

ItalStructures, Riva Del Garda, Italy. The XRD patterns were recorded over the 5–80° 2θ range with a 2θ step of 0.025 or 0.05° and a counting time per step of 15–40 s.

^{57}Fe Mössbauer spectra were recorded at 20 °C in the transmission mode using a standard instrumental configuration by WissEl GmbH (Starnberg, Germany). The ^{57}Co in the rhodium matrix was used as a Mössbauer source. The spectrometer was calibrated at 20 °C using the standard α-Fe foil spectrum. The velocity scale and all the data refer to the metallic α-Fe absorber at 20 °C. The experimentally observed Mössbauer spectra were fitted using the MossWinn program.

2.4. Determination of Fe^{2+} in γ-irradiated suspensions by potassium permanganate titration

2.4.1. Chemicals for permanganate titration

Potassium permanganate solution (0.02 M, standardized against oxalate) supplied by Merck, hydrochloric acid (fuming, ≥37 wt%) by *Fluka;* manganese(II) sulfate monohydrate (p.a. EMSURE, ACS, reag. Ph. Eur.) by *Merck*, ortho-phosphoric acid (85% p.a.) by *LachNer*, sulfuric acid (96%, p.a.) by *LachNer*, tin(II) chloride dehydrate (p.a., EMSURE, ACS, ISO, Reag. Ph. Eur.) by *Merck* and mercury(II) chloride (analytical reagent grade) supplied by *Fisher Scientific* were used.

2.4.2. Potassium permanganate titration

In order to determine the Fe^{2+} concentration in γ-irradiated suspensions the permanganate titration procedure was performed. Immediately after irradiation, concentrated hydrochloric acid (2.5 mL of 37 wt% HCl solution) was added by syringe through rubber septa to 100 mL of γ-irradiated suspensions in order to dissolve all formed precipitates and lower the pH to slightly below 1. At such low pH a clear solution formed that preserved all Fe^{2+} formed upon γ-irradiation. Furthermore, at such low pH the Fe^{2+} ions are not able to oxidize to Fe^{3+}. Then, the γ-irradiated solutions were titrated with 0.02 M potassium permanganate solution following the standard permanganate titration procedure (with the addition of Zimmermann-Reinhardt solution). The Fe^{2+} concentration formed on γ-irradiation was determined, as well as total iron concentration. To check the total iron concentration the remaining Fe^{3+} (not reduced by γ-irradiation) was reduced with tin(II) chloride, and small excess of $SnCl_2$ was treated with mercury(II) chloride, prior to titration.

3. Results and discussions

In this work, the iron(III) chloride aqueous colloidal solutions (pH ≅ 9) in the presence of 2-propanol and dextran sulfate were deoxygenated by nitrogen and then γ-irradiated at doses of 36 and 130 kGy. The addition of 2-propanol and bubbling with nitrogen gas emphasized the reducing conditions upon γ-irradiation [15–18,27,28]. The dose of 36 kGy was selected because we experimentally found that at this dose magnetite could be obtained. The dose of 130 kGy was selected because in previous works at about this dose we unexpectedly obtained δ-FeOOH nanodiscs [19]. Furthermore, we observed that the white suspension characteristic of $Fe(OH)_2$ was formed, which after coming in contact with air turned to a green-gray suspension characteristic of Green Rust. These Fe(II) intermediate products are extremely susceptible to oxidation and they have not been experimentally confirmed in our previous work [19]. Due to these reasons in this work the special attention is devoted to the isolation of the γ-irradiated samples.

Fig. 2 shows the XRD patterns of conventionally isolated samples (washing with water/centrifugation). Sample S-130W1 was aged one day prior to the isolation. The XRD pattern of sample S-36W matches best with the patterns of Green Rust II ($GR(SO_4^{2-})$), schwertmannite [43,44] (ideal chemical formula $Fe_8O_8(OH)_6(SO_4)\cdot nH_2O$), feroxyhyte (δ-FeOOH) and lepidocrocite (γ-FeOOH).

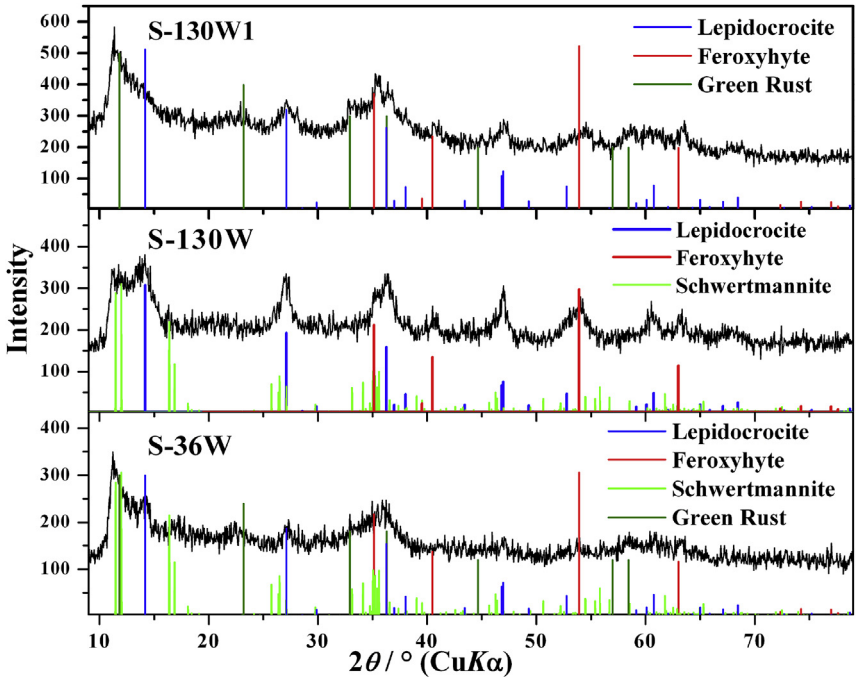

Fig. 2. XRD patterns of samples S-36W, S-130W and S-130W1. The XRD pattern of sample S-36W agrees best with the patterns of Green Rust (card no. 13-0090), schwertmannite [43], feroxyhyte (card no. 77-0247) and lepidocrocite, (card no. 70-0714). Sample S-130W matches best with the patterns of schwertmannite [43], feroxyhyte (card no. 77-0247) and lepidocrocite, (card no. 70-0714). Sample S-130W1 matches best with the patterns of Green Rust (card no. 13-0090), feroxyhyte (card no. 77-0247) and lepidocrocite (card no. 70-0714).

Sample S-130W agrees best with the patterns of schwertmannite, feroxyhyte and lepidocrocite, while sample S-130W1 matches best with the patterns of GR(SO_4^{2-}), feroxyhyte and lepidocrocite. The volume average domain sizes were estimated using Scherrer equation:

$$D_{hkl} = \frac{0.9\lambda}{\beta hkl \times \cos\theta}, \quad (1)$$

where D_{hkl} is a volume average of the crystal thickness in the direction normal to the reflecting planes (*hkl*), λ is the x-ray wavelength (Cu*K*α), θ is the Bragg angle and β_{hkl} is pure full width of the diffraction line (*hkl*) at half the maximum intensity.

The volume average domain sizes of the 003 lines (D_{003}) of Green Rust in sample S-130W1 were estimated to ~8.3 nm. The D_{021} of lepidocrocite (γ-FeOOH) in samples S-36W, S-130W and S-130W1 were estimated to ~10.1, ~8.7 and ~5.5 nm, respectively. The D_{100} of δ-FeOOH in sample S-130W1 was estimated to ~11.2 nm (Table 2).

Fig. 3 shows the Mössbauer spectra of samples S-130W1, S-130W and S-36W recorded at 20 °C. The PD and/or SP doublet D1 is due to Fe(III) paramagnetic and/or superparamagnetic nanoparticles. The sextet M1 is assigned to δ-FeOOH in line with the XRD results. Sample S-130W1 is characterized with additional doublet D2 ($\Delta = 2.69$ mm s^{-1}) due to the high spin Fe(II) in GR(SO_4^{2-}) [34,35,37]. The calculated amount of Fe(II) is 5.7% (Table 3).

Table 2
The *hkl* indices, the 2θ positions, the full width at half maximum (FWHM) values and the D_{hkl} values (estimated from Scherrer equation) of the most prominent diffraction lines of γ-FeOOH (lepidocrocite), δ-FeOOH (feroxyhyte) and GR(SO_4^{2-}) in selected samples.

Sample	Phase	*hkl*	2θ/°	FWHM/°	D_{hkl}/nm
S-36W	γ-FeOOH	021	27.1	0.91	~10.1
S-130E	δ-FeOOH	100	35.1	0.36	~26.1
S-130E1	δ-FeOOH	100	35.1	0.53	~17.2
S-130W	γ-FeOOH	021	27.1	0.74	~12.0
S-130W1	GR(SO_4^{2-})	003	11.8	1.10	~8.3
	γ-FeOOH	021	27.1	1.68	~5.5
	δ-FeOOH	100	35.1	0.82	~11.2

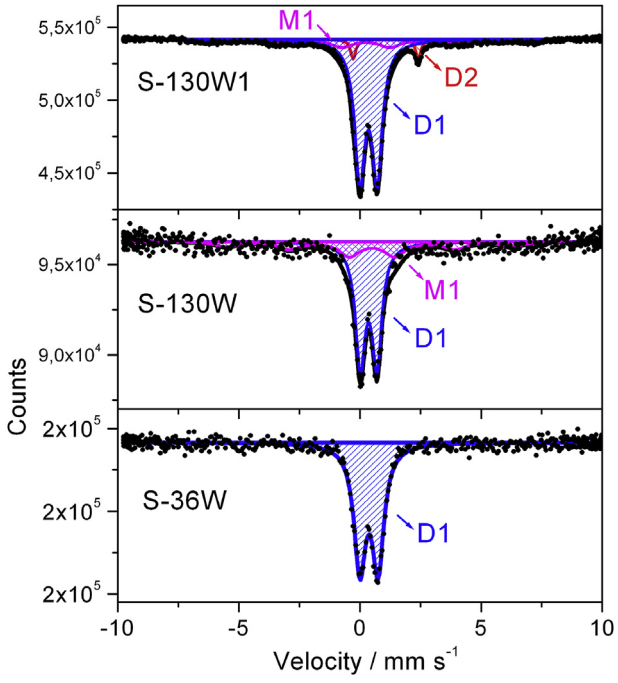

Fig. 3. Mössbauer spectra of samples S-130W1, S-130W and S-36W recorded at 20 °C.

Contrary to the washing with water, we assume that rinsing with ethanol should produce samples in a more reduced state. Ethanol is frequently used for isolation of samples susceptible to oxidation. For instance, ethanol was used for isolation of magnetite [16] and zero-valent iron NPs [45]. Fig. 4 shows XRD patterns of samples S-36E, S-130E and S-130E1 that were isolated in the presence of ethanol. The XRD pattern of sample S-36E matched best with the patterns of magnetite (Fe_3O_4) and GR(SO_4^{2-}). Sample S-130E and sample 130E1 agree best with the patterns of iron(III) sulfate hydroxide (ideal chemical formula ($Fe_4(OH)_{10}SO_4$)), feroxyhyte and goethite (α-FeOOH). The XRD pattern of sample S-130E1 possesses the additional lines indicated with asterisks that belong to an unidentified phase. The average crystallite sizes of the 100 line of δ-FeOOH in samples S-130E and S-130E1 (D_{100}) were estimated to ~26.1 and ~17.2 nm, respectively.

Fig. 5 shows the Mössbauer spectra of samples S-130E1, S-130E and S-36E recorded at 20 °C. Sample S-36E is characterized with PD and/or SP doublet D1 that belongs to the paramagnetic Fe(III) and/or superparamagnetic small non-stoichiometric magnetite NPs. The Δ of 0.80 mm s^{-1} suggests the presence of very small crystallites in this sample.

Sample S-130E is a superposition of two sextets M1 and M2 and a doublet D1. The sextet M1 with smaller hyperfine magnetic field ($B_{hf} = 27.29$ T) is assigned to α-FeOOH, whereas the sextet M2 with $B_{hf} = 37.84$ T is assigned to δ-FeOOH. These assignations are in line with XRD results that showed much broader goethite XRD lines in comparison to the feroxyhyte XRD lines. The Δ of PD and/or SP doublet D1 confirms the presence of very small crystallites in this sample. Generally, the room temperature Mössbauer spectrum of goethite may vary from a well-shaped sextet down to a paramagnetic/superparamagnetic doublet, which depends on the size and crystallinity of the goethite particles.

Sample S-130E1 is characterized with SP and/or PD doublet D1 with high quadrupole splitting (Δ) of 0.80 mm s^{-1} due to the very small crystallites in this sample. The sextet M3 that is of low intensity and very broaden ($\Gamma = 1.38$ mm s^{-1}) is assigned to both α-FeOOH and δ-FeOOH.

The conventionally isolated samples in the presence of water contained exclusively Fe(III) products, whereas the ethanol-isolated samples contained insignificant amount of iron(II) phases. The samples washed with water consisted of γ-FeOOH (lepidocrocite), δ-FeOOH (feroxyhyte) and schwertmannite (iron-oxyhydroxysulfate mineral with an ideal chemical formula of $Fe_8O_8(OH)_6(SO_4)\cdot nH_2O$. Instead of schwertmannite, GR(SO_4^{2-}) was found in sample S-130W1. The lack of iron(III) sulfate hydroxide in the samples washed with water could be explained by different solubility of sulfate in ethanol versus water (see Figs. S3 and S4 in Supplementary materials). Thus, the high solubility of sulfate in water favored the precipitation of γ-FeOOH and schwertmannite, whereas the low solubility of sulfate during isolation with ethanol favored the precipitation of α-FeOOH (goethite) and iron(III) hydroxide sulfate ($Fe_4(OH)_{10}SO_4$). In addition, γ-FeOOH and α-FeOOH can be synthesized starting from iron(III) precursor, however, δ-FeOOH synthesis always starts from iron(II) precursors. Thus, in order to ascertain the formation of iron(II) phases the samples were isolated by admixing glycerol. In this way, glycerol that contains hydroxyl groups retarded the oxidation of otherwise very oxidation-sensitive compounds [46].

Fig. 6 shows the XRD patterns of samples S-130U, S-36G and S-130G. The samples S-36G and S-130G were isolated by admixing glycerol, whereas the sample S-130U was isolated by centrifugation without washing or admixing glycerol. The XRD lines are broad due

Table 3
^{57}Fe Mössbauer parameters calculated for selected samples at 20 °C.

Sample	Fitting curve	Δ (mm s^{-1})	Δ or 2ε (mm s^{-1})	B_{hf} (T)	Γ (mm s^{-1})	Relative area (%)	Assignations	Σ Fe(II) (%)	χ^2
S-130W1	D1	0.35	0.72		0.51	77.9	Fe(III), SP and/or PD	5.7	1.56
	D2	1.06	2.69		0.26	5.7	Fe(II) in GR(SO_4^{2-})		
	M1	0.30	0.10	38.81	1.00*	16.4	δ-FeOOH		
S-130W	D1	0.36	0.68		0.49	68.6	Fe(III), SP and/or PD		1.10
	M1	0.43	−0.13	36.55	1.00*	31.4	δ-FeOOH		
S-36W	D1	0.37	0.75		0.59	100.0	Fe(III), SP and/or PD	–	1.24
S-130E1	D1	0.35	0.80		0.44	62.9	Fe(III), SP and/or PD	–	1.07
	M3	0.30	−0.06	37.96	1.38	37.1	δ-FeOOH and α-FeOOH		
S-130E	D1	0.35	0.75		0.51	40.9	Fe(III), SP and/or PD	–	1.33
	M1	0.31	−0.11	27.29	1.30*	34.4	α-FeOOH		
	M2	0.33	0.09	37.84	1.05*	24.7	δ-FeOOH		
S-36E	D1	0.37	0.80		0.46	100.0	Fe(III), SP and/or PD	–	0.96
S-130G	D1	0.45	0.56		0.59*	17.3	Fe(III) and/or Fe(II)S_{1-x}	82.6	1.10
	D2	1.12	2.43		0.45*	26.6	Fe(II) in GR(SO_4^{2-})		
	D3	1.14	2.98		0.33	56.0	Fe(II) in $Fe(OH)_2$		
S-36G	D1	0.35	0.47		0.55*	39.5	Fe(III) and/or Fe(II) sulfide	60.5	1.17
	D2	1.10	2.47		0.46	60.5	Fe(II) in GR(SO_4^{2-})		
S-130U	D1	0.36	0.73		0.52	64.3	Fe(III), PD and/or SP	7.2	1.69
	D3	1.07	2.68		0.37	7.2	Fe(II) in $Fe(OH)_2$ and GR(SO_4^{2-})		
	M1	0.34	0.11	35.27	1.00*	28.5	δ-FeOOH		

Key: δ = isomer shift given relative to α-Fe at 20 °C; Δ or 2ε = quadrupole splitting (doublets) or quadrupole shift (sextets); B_{hf} = hyperfine magnetic field; Γ = line width; **Σ Fe(II)** = Fe(II) in total. Error: $\delta = \pm 0.01$ mm s^{-1}; Δ or $2\varepsilon = \pm 0.01$ mm s^{-1}; $B_{hf} = \pm 0.2$ T.
Remarks: PD = paramagnetic doublet; SP = superparamagnetic doublet; M1 = sextet due to the hyperfine magnetic fields; * = fixed; Σ = in total.

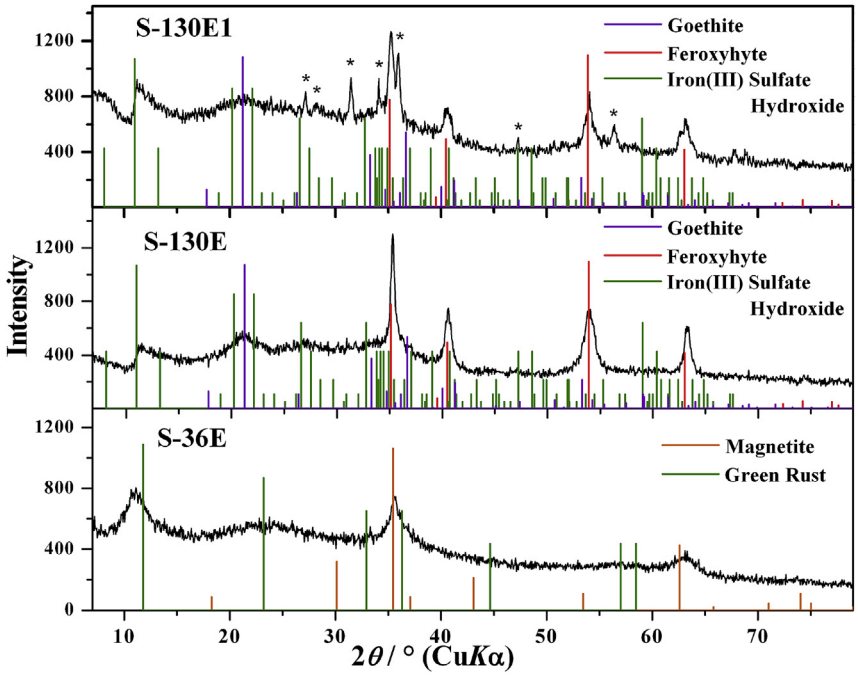

Fig. 4. XRD patterns of samples S-36E, S-130E and S-130E1. The XRD patterns of sample S-36E match best with the patterns of magnetite (card no. 19-0629), Green Rust (card no. 13-0090). Sample S-130E and sample 130E1 match best with the patterns of iron(III) sulfate hydroxide, [$Fe_4(OH)_{10}(SO_4)$], (card no. 21-0429), feroxyhyte (card no. 77-0247) and goethite (card no. 29-0713). The XRD patterns of sample S-130E1 possess the additional lines indicated with asterisks that belong to unidentified phase.

to the small crystallite size and presence of amorphous phases. The XRD pattern of sample S-130U matches best with the patterns of iron(II) hydroxide ($Fe(OH)_2$), iron oxide sulfate hydroxide also called Green Rust II (GR(SO_4^{2-}), ideal chemical formula Fe(II)$_4$-Fe(III)$_2$(OH)$_{12}$SO$_4$·8H$_2$O, and feroxyhyte. Sample S-36G agrees best with the patterns of GR(SO_4^{2-}), iron carbonyl sulfide and chaoite, whereas sample S-130G matches best with the patterns of mackinawite (FeS_{1-x}), GR(SO_4^{2-}) and $Fe(OH)_2$.

Fig. 7 shows the Mössbauer spectra of samples S-130G, S-36G and S-130U recorded at 20 °C. Sample S-130G is fitted to the three doublets D1, D2 and D3. The doublet D3 with isomer shift (δ) of 1.14 mm s^{-1} and quadrupole splitting (Δ) of 2.98 mm s^{-1} is assigned to Fe(II) in $Fe(OH)_2$, whereas the doublet D2 ($\delta = 1.12$ mm s^{-1} and $\Delta = 2.43$ mm s^{-1}) is due to high spin Fe(II) ions in octahedral sites of GR(SO_4^{2-}). In line with the XRD results, the doublet D1 with a small quadrupole splitting ($\Delta = 0.56$ mm s^{-1}) can be assigned to high spin Fe(III) ions in GR(SO_4^{2-}) and/or to low spin Fe(II) in mackinawite, iron (II) sulfide, FeS_{1-x} [47]. The relative amount of Fe(II) was determined on the basis of doublets D2 and D3 (82.6%, Table 3).

Sample S-36G is fitted to the two doublets. The outer doublet D2 with the $\delta = 1.10$ mm s^{-1} and $\Delta = 2.47$ mm s^{-1} is due to the high

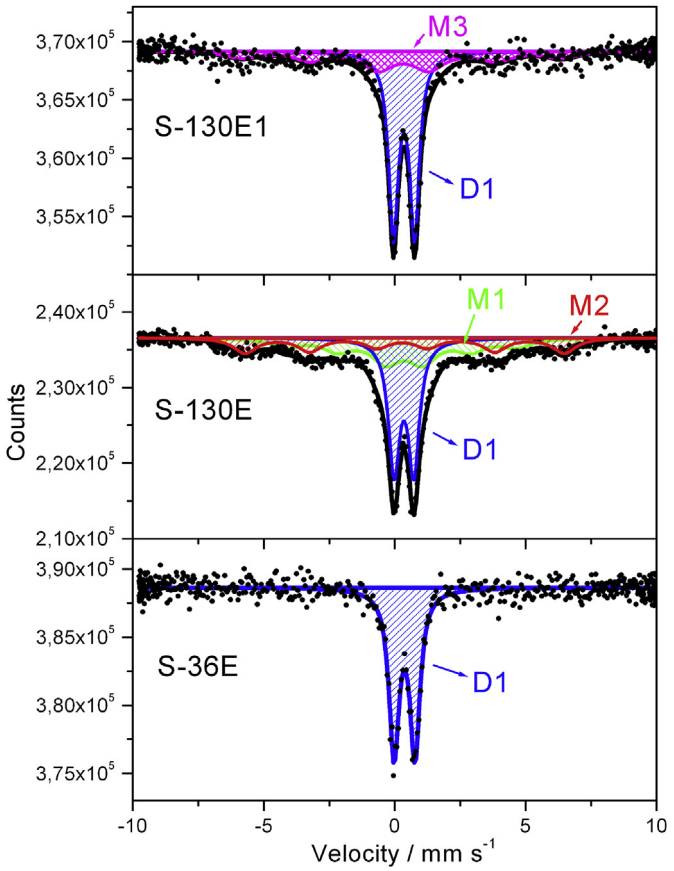

Fig. 5. Mössbauer spectra of samples S-130E1, S-130E and S-36E recorded at 20 °C.

spin Fe(II) ions in GR(SO_4^{2-}). The XRD results and the line width (Γ) of 0.46 mm s^{-1} suggest that sample S-36G contains no $Fe(OH)_2$. Likewise in sample S-130G, the inner doublet D1 can be assigned to the high spin Fe(III) in GR(SO_4^{2-}) and tentatively, to the low spin Fe(II) in iron carbonyl sulfide, the phase which was observed by XRD. The relative amount of Fe(II) was determined on the basis of only outer doublet D2 that gave the value of 60.5% of Fe(II) in sample S-36G (Table 3).

The Mössbauer spectrum of irradiated unwashed sample, sample S-130U, is fitted to the two doublets D1 and D3 and a sextet M1. The sextet M1 with hyperfine magnetic field (B_{hf}) of 35.27 T, quadrupole shift (2ε) of 0.11 mm s^{-1} and δ of 0.34 mm s^{-1} is assigned to δ-FeOOH (feroxyhyte). δ-FeOOH is magnetic at room temperature and that is why sample S-130U was attracted by magnet (Table 1). In line with XRD results, the outer doublet D3 is attributed to the Fe(II) in $Fe(OH)_2$ and GR(SO_4^{2-}). The amount of Fe(II) in sample S-130U calculated on the basis of D3 doublet is 7.2% (Table 3). The inner doublet D1 is due to the presence of high spin Fe(III) in paramagnetic and/or superparamagnetic state (PD and/or SP doublet). The time scale of measurements in Mössbauer spectroscopy is an order of nanoseconds, which allows Mössbauer spectroscopy to observe the fast spin relaxation processes in nanoparticles caused by the thermal energy [1,16,17,48]. The particle size has a strong influence on the Mössbauer parameters because magnetically ordered materials in the form of very small particles (about 10 nm in size) exhibit paramagnetic or superparamagnetic behavior. The superparamagnetic (magnetic moments related to the single domains that may contain 10^5 or more atoms) and paramagnetic (magnetic moments related to the individual atoms) nanoparticles show doublets in the Mössbauer spectrum at room temperature. This is because at this relatively high temperature the thermal fluctuations become larger and more

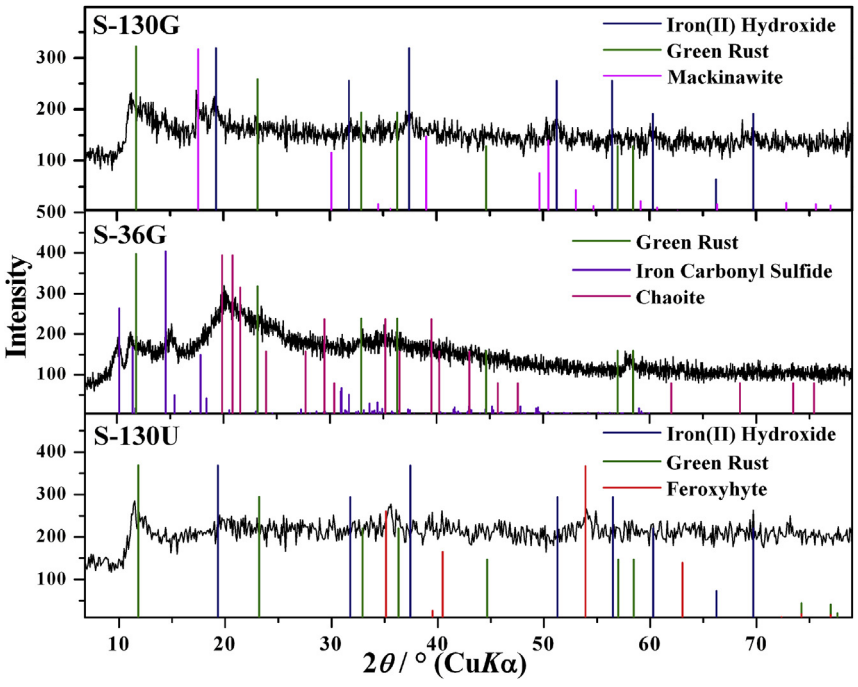

Fig. 6. XRD patterns of samples S-130U, S-36G and S-130G. The XRD patterns of sample S-130U match best with the patterns of iron(II) hydroxide ($Fe(OH)_2$, card no. 13-0089), Green Rust (card no. 13-0090) and feroxyhyte (δ-FeOOH, card no. 77-0247). Sample S-36G agrees best with the patterns of chaoite (card no. 22-1069), iron carbonyl sulfide (card no. 80-2195), Green Rust (card no. 13-0089). Sample S-130G matches best with the patterns of mackinawite (FeS_{1-x}, card no. 86-0389), Green Rust (card no. 13-0090) and iron(II) hydroxide (card no. 13-0089).

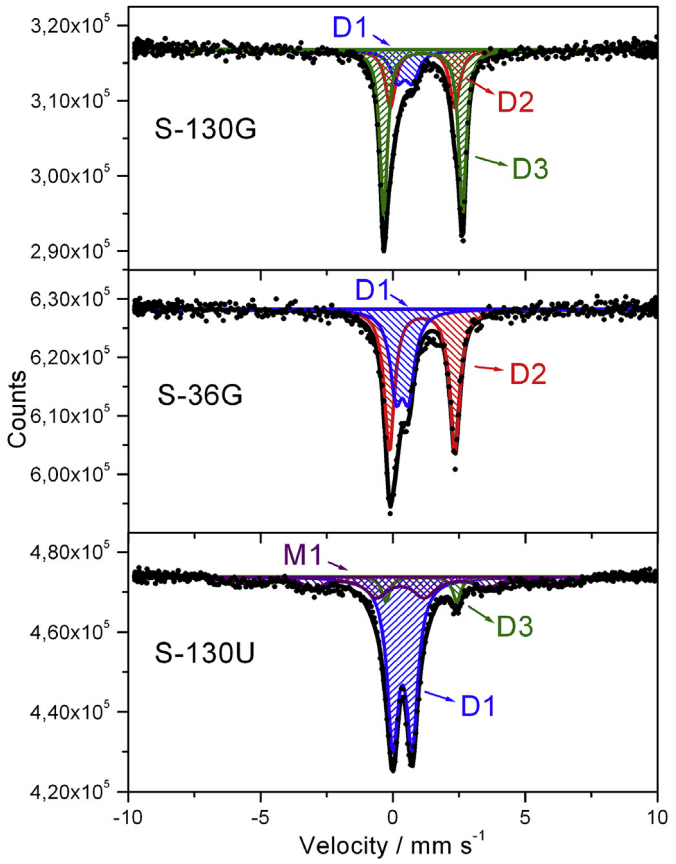

Fig. 7. Mössbauer spectra of samples S-130G, S-36G and S-130U recorded at 20 °C. The Mössbauer parameters and assignations for fitted doublets D1 to D3 and sextet M1 are given in Table 3. The doublets D2 and D3 are associated with Fe(II). The calculated relative amounts of Fe(II) in samples S-130G, S-36G and S-130U were 82.6, 60.5 and 7.2%, respectively.

frequent, which causes the direction of magnetization to undergo random reorientation. In addition, the high values of quadrupole splitting that are greater than 0.70 mm s^{-1} ($\Delta > 0.7$ mm s^{-1}) suggest that the sample consists of very small crystallites. These small crystallites have a large surface to volume ratio, which increases the lattice strain and consequently, causes a large electric field gradient at the iron nuclei [48]. Thus, the doublet D1 with $\Delta = 0.73$ mm s^{-1} suggests the presence of very small crystallites in sample S-130U.

The relative amounts of Fe(II) in solid samples were determined by Mössbauer spectroscopy. Samples S-36G and S-130G contained 60.5% and 82.6% of Fe(II), respectively (Tables 1 and 3). The concentrations of Fe^{2+} in the acidified solutions containing dissolved γ-irradiation products were determined using potassium permanganate titrations. The amounts of Fe^{2+} in the solutions were 72.0% and 92.0% at doses of 36 and 130 kGy, respectively (Table 3). Therefore, comparing the isolations by water, ethanol and glycerol the reducing conditions were preserved to the highest degree by admixing glycerol. Sample S-36 consisted of hydroxysulfate green rust II [GR(SO_4^{2-})] whereas sample S-130G consisted of $Fe(OH)_2$, GR(SO_4^{2-}) and nonstoichiometric FeS_{1-x} (mineral name Mackinawite). Mackinawite [47] is a metastable mineral that precipitates in aqueous environments at low temperatures (around room temperature). Green Rusts (GRs) [34–39,49] belongs to the layered double hydroxides. Structurally, GRs contain both Fe(II) and Fe(III) cations in brucite-like layers along with intercalated anions. Most common types of GRs are hydroxysulfate GR II [GR(SO_4^{2-})] and hydroxycarbonate GR I [GR(CO_3^{2-})] according to the type of intercalated anions [i.e., sulfate (SO_4^{2-}) or carbonate (CO_3^{2-}), respectively]. The ideal chemical formula of GR(SO_4^{2-}) is $Fe(II)_4Fe(III)_2(OH)_{12}SO_4 \cdot 8H_2O$ [49].

Fig. 8 shows SEM images of samples S-36E, S-130E, S-130U and S-130E1. The sample S-36E consisted of aggregates with platelike particles. The sample S-130E consisted of very big aggregates with no visible discrete nanoparticles. The samples 130E1 and S-130U consist of large aggregates; also big irregular plate-like particles are

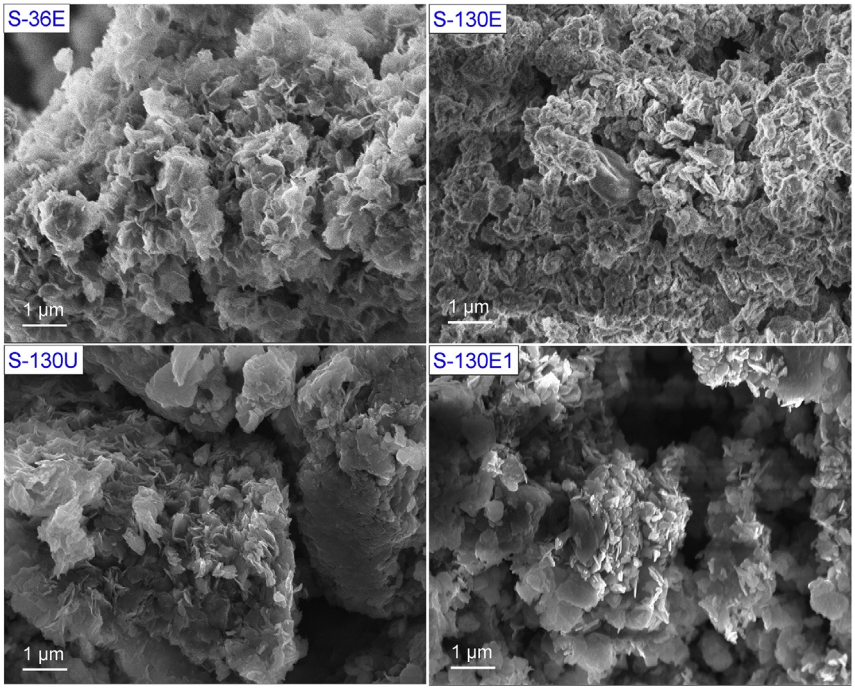

Fig. 8. SEM images of samples S-36E, S-130E, S-130U and S-130E1.

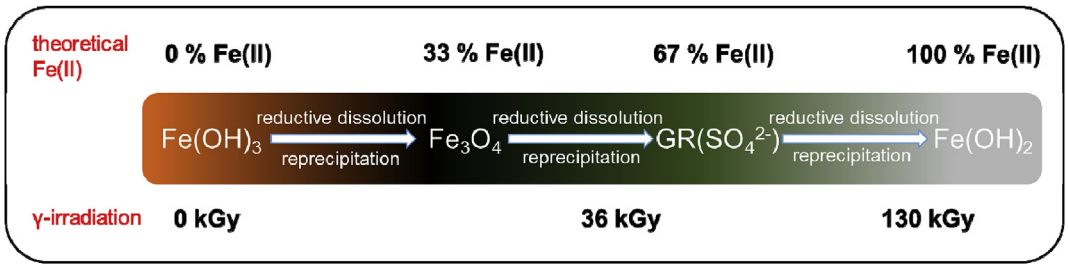

Fig. 9. The simplified scheme of the transformations that proceeded upon γ-irradiation of deoxygenated Fe(III) alkaline aqueous precursor in the presence of 2-propanol and dextran sulfate.

visible that emerge from the bulk. The SEM images with EDS analyses of other synthesized samples are given in Supplementary materials. Generally, the synthesized samples mostly consisted of particles aggregates with no visible discrete nanoparticles. This may be due to the high agglomerations of small nanoparticles during the isolation of powder samples from irradiated suspensions. The EDS analyses shows that particles contained sulfur (S), which is in line with iron sulfur (oxy)hydroxide phases identified by XRD.

Based on the above presented results the γ-irradiation initiated the following sequence of reactions as shown in Fig. 9.

γ-irradiation in a series of reactions reductively dissolves Fe(III), which re-precipitates as Fe_3O_4, $GR(SO_4^{2-})$, $Fe(OH)_2$ and FeS_{1-x}. However, after the vial cap has been opened and the γ-irradiated suspensions have come into contact with air the Fe(II)-products readily oxidized. The degree of oxidation is proportional to the relative content of Fe(II). For instance, γ-irradiation of "$Fe(OH)_3$" precursor (see Fig. S5 in Supplementary Materials) with dose of 130 kGy generated almost 100% of Fe^{2+}, whereas the isolated products consisted exclusively of Fe(III). Therefore, on the basis of isolated Fe(III) products one can not conclude about the real reducing conditions produced upon γ-irradiation. The main reason is the high reactivity of Fe(II)-rich precipitates that completely oxidized to Fe(III) products. The more information about the γ-irradiation-induced chemical changes to iron oxides can be found in Refs. [29,50–53].

The formation of iron(II) sulfide, *i.e.* sulfur deficient mineral mackinawite (FeS_{1-x}) in sample S-130G can be explained by analogy to its formation in nature [36,54]. Mackinawite is authigenic mineral that precipitates in shallow-water marine sediments. In a simple model, organic carbon is assumed to be in the form of a carbohydrate ("CH_2O") that represents the reduced form of carbon. In saline anoxic layers of estuarine and coastal environments, the carbohydrate reduces insoluble iron(III) oxyhydroxides to soluble Fe^{2+} and sulfate anions (SO_4^{2-}) to sulfides (S^{2-}). Sulfates are major constituents of seawater and at high salinity and at high sulfate reduction rate the H_2S buildup. The high concentrations of dissolved Fe^{2+} and HS^- in the alkaline solution such as seawater lead to the precipitation of mackinawite [54]. Mackinawite is metastable and it re-oxidizes again to iron(III) oxyhydroxide and sulfates. In this work, we unintentionally mimicked the environmental conditions for the formation of mackinawite, however, instead of seawater we used the alkaline solution and instead of carbohydrate and sulfates we used dextran sulfate. Besides, the "$Fe(OH)_3$" precursor we used in this work is very similar to the low-crystalline iron (oxy)hydroxide phases found in the marine sediments.

Finally, the formation of carbon and sulfide phases such as iron carbonyl sulfide, Chaoite (white carbon) and FeS_{1-x} (Mackinawite) (Fig. 6) suggests that dextran sulfate plays an active role in the γ-irradiation synthesis of magnetic iron oxide phases. The same as Fe(III) precursor, the dextran sulfate was involved in complex oxidation-reduction reactions, however, in this study the focus is on the synthesis and characterization of iron oxide phases, whereas the characterization of radiolytic products directly related to the dextran sulfate requires different characterization techniques and methodologies that are out of scope of this study.

4. Conclusions

In this work, the impact of dextran sulfate on the radiolytical synthesis of magnetic iron oxides NPs was studied. The deoxygenated iron(III) chloride alkaline aqueous colloidal solutions in the presence of 2-propanol and dextran sulfate polymer were γ-irradiated with doses of 36 and 130 kGy. The dose rate was ~31 kGy h^{-1}.

The samples collected by washing with water mainly consisted of γ-FeOOH (lepidocrocite), δ-FeOOH (feroxyhyte) and schwertmannite (iron-oxyhydroxysulfate mineral with an ideal chemical formula of $Fe_8O_8(OH)_6(SO_4)\cdot nH_2O$). The different iron oxyhydroxide and hydroxysulfate phases found in the samples washed with ethanol versus water could be explained by high solubility of sulfate in water that favored the precipitation of lepidocrocite and schwertmannite, whereas the low solubility of sulfate in ethanol during isolation favored the precipitation of goethite and iron(III) hydroxide sulfate.

The samples isolated by rinsing with ethanol mainly consisted of iron(III) oxidized phases: α-FeOOH (goethite), δ-FeOOH (feroxyhyte) and iron(III) hydroxide sulfate ($Fe_4(OH)_{10}SO_4$). At lower dose (36 kGy) magnetite was formed.

The samples isolated by admixing glycerol consisted of intermediate phases $Fe(OH)_2$, $GR(SO_4^{2-})$ and non-stoichiometric FeS_{1-x} (mineral name mackinawite). The total amounts of Fe(II) in isolated solid samples were determined using Mössbauer spectroscopy. The 60.5% and 82.6% of Fe(II) were found at dose of 36 and 130 kGy, respectively. Moreover, the amounts of Fe^{2+} in the acidified solutions containing dissolved γ-irradiation products were determined by potassium permanganate titration. The amounts of Fe^{2+} in the solutions were 72.0% and 92.0%., which are in very good agreement with the Fe(II) values determined by Mössbauer spectroscopy. The unwashed sample has 7% of iron(II) and consisted of $Fe(OH)_2$, $GR(SO_4^{2-})$ and δ-FeOOH.

Thus, although the conventionally isolated samples consisted of Fe(III) products, the reducing conditions of γ-irradiation were confirmed by isolation of Fe(II) intermediate phases and quantitative determinations of Fe(II) and Fe^{2+}. Obviously, the phase composition of the radiolytically obtained products depends not only on the applied dose, but also on the way of powder sample isolation. The reducing conditions generated upon γ-irradiation were preserved to the highest degree by admixing glycerol.

Admixing glycerol can be used as a general tool for isolation of intermediate products susceptible to oxygen.

Acknowledgements

This work has been supported by Croatian Science Foundation under the project UIP-2017-05-7337 "The impact of polymers on the radiolytic synthesis of magnetic nanoparticles" (acronym: POLRADNANOP).

Appendix A. Supplementary data

Supplementary data to this article can be found online at https://doi.org/10.1016/j.molstruc.2019.01.075.

References

[1] R.M. Cornell, U. Schwertmann, The Iron Oxides: Structure, Properties, Reactions, Occurrences, and Uses, 2nd, Wiley-VCH, Weinheim, 2003 completely rev. and extended ed.
[2] M. Gotić, S. Popović, S. Musić, Formation and characterization of δ-FeOOH, Mater. Lett. 21 (1994) 289–295, https://doi.org/10.1016/0167-577X(94)90192-9.
[3] M. Gotić, S. Popović, N. Ljubešić, S. Musić, Structural properties of precipitates formed by hydrolysis of Fe^{3+} ions in aqueous solutions containing NO_3^- and Cl^- ions, J. Mater. Sci. 29 (1994) 2474–2480, https://doi.org/10.1007/BF00363442.
[4] S. Musić, S. Popović, M. Gotić, Mössbauer spectroscopy and X-ray diffraction of oxide precipitates formed from FeSO4 solution, J. Mater. Sci. 25 (1990) 3186–3190, https://doi.org/10.1007/BF00587672.
[5] G. Dražić, G. Štefanić, T. Jurkin, M. Gotić, Impact of cadmium and phosphate ions on the hematite nanorings formation, J. Mol. Struct. 1140 (2017) 113–121, https://doi.org/10.1016/J.MOLSTRUC.2016.12.089.
[6] M. Gotić, G. Dražić, S. Musić, Hydrothermal synthesis of α-Fe_2O_3 nanorings with the help of divalent metal cations, Mn^{2+}, Cu^{2+}, Zn^{2+} and Ni^{2+}, J. Mol. Struct. 993 (2011) 167–176, https://doi.org/10.1016/J.MOLSTRUC.2010.12.063.
[7] S. Ivanković, M. Gotić, M. Jurin, S. Musić, Photokilling squamous carcinoma cells SCCVII with ultrafine particles of selected metal oxides, J. Sol. Gel Sci. Technol. 27 (2003) 225–233, https://doi.org/10.1023/A:1023715004575.
[8] M. Gotić, G. Koščec, S. Musić, Study of the reduction and reoxidation of substoichiometric magnetite, J. Mol. Struct. 924–926 (2009) 347–354, https://doi.org/10.1016/J.MOLSTRUC.2008.10.048.
[9] S. Musić, S. Popović, M. Gotić, Mossbauer spectroscopy and X-ray diffraction of oxide precipitates formed from FeSO4 solution. Part II, Croat. Chem. Acta 60 (1987) 661–675.
[10] M. Gotić, S. Musić, S. Popović, L. Sekovanić, Investigation of factors influencing the precipitation of iron oxides from Fe (II) containing solutions, Croat. Chem. Acta 81 (2008) 569–578.
[11] N. Šijaković-Vujičić, M. Gotić, S. Musić, M. Ivanda, S. Popović, Synthesis and microstructural properties of Fe-TiO_2 nanocrystalline particles obtained by a modified sol-gel method, J. Sol. Gel Sci. Technol. 30 (2004) 5–19, https://doi.org/10.1023/B:JSST.0000028174.90247.a9.
[12] M. Gotić, S. Musić, Synthesis of nanocrystalline iron oxide particles in the iron(III) acetate/alcohol/acetic acid system, Eur. J. Inorg. Chem. (2008) 966–973, https://doi.org/10.1002/ejic.200700986 (2008).
[13] M. Gotić, S. Musić, Mössbauer, FT-IR and FE SEM investigation of iron oxides precipitated from $FeSO_4$ solutions, J. Mol. Struct. 834–836 (2007) 445–453, https://doi.org/10.1016/J.MOLSTRUC.2006.10.059.
[14] J. Fan, Z. Zhao, Z. Ding, J. Liu, Synthesis of different crystallographic FeOOH catalysts for peroxymonosulfate activation towards organic matter degradation, RSC Adv. 8 (2018) 7269–7279, https://doi.org/10.1039/C7RA12615H.
[15] M. Gotić, T. Jurkin, S. Musić, Factors that may influence the micro-emulsion synthesis of nanosize magnetite particles, Colloid Polym. Sci. 285 (2007) 793–800, https://doi.org/10.1007/s00396-006-1624-2.
[16] M. Gotić, T. Jurkin, S. Musić, From iron(III) precursor to magnetite and vice versa, Mater. Res. Bull. 44 (2009) 2014–2021, https://doi.org/10.1016/J.MATERRESBULL.2009.06.002.
[17] T. Jurkin, K. Zadro, M. Gotić, S. Musić, Investigation of solid phase upon γ-irradiation of ferrihydrite-ethanol suspension, Radiat. Phys. Chem. 80 (2011) 792–798, https://doi.org/10.1016/J.RADPHYSCHEM.2011.02.031.
[18] T. Jurkin, M. Gotić, G. Štefanić, I. Pucić, Gamma-irradiation synthesis of iron oxide nanoparticles in the presence of PEO, PVP or CTAB, Radiat, Phys. Chem. 124 (2016) 75–83, https://doi.org/10.1016/J.RADPHYSCHEM.2015.11.019.
[19] T. Jurkin, G. Štefanić, G. Dražić, M. Gotić, Synthesis route to δ-FeOOH nanodiscs, Mater. Lett. 173 (2016) 55–59, https://doi.org/10.1016/J.MATLET.2016.03.009.
[20] S. Wang, H. Xin, Y. Qian, Preparation of nanocrystalline Fe_3O_4 by γ-ray radiation, Mater. Lett. 33 (1997) 113–116, https://doi.org/10.1016/S0167-577X(97)00077-3.
[21] S. Wang, H. Xin, The γ-irradiation-induced chemical change from β-FeOOH to Fe_3O_4, Radiat. Phys. Chem. 56 (1999) 567–572, https://doi.org/10.1016/S0969-806X(99)00319-9.
[22] A. Aqil, S. Vasseur, E. Duguet, C. Passirani, J.P. Benoît, A. Roch, R. Müller, R. Jérôme, C. Jérôme, PEO coated magnetic nanoparticles for biomedical application, Eur. Polym. J. 44 (2008) 3191–3199, https://doi.org/10.1016/J.EURPOLYMJ.2008.07.011.
[23] K.M. Koczkur, S. Mourdikoudis, L. Polavarapu, S.E. Skrabalak, Polyvinylpyrrolidone (PVP) in nanoparticle synthesis, Dalt. Trans. 44 (2015) 17883–17905, https://doi.org/10.1039/C5DT02964C.
[24] H. Pardoe, W. Chua-anusorn, T.G.St Pierre, J. Dobson, Structural and magnetic properties of nanoscale iron oxide particles synthesized in the presence of dextran or polyvinyl alcohol, J. Magn. Magn Mater. 225 (2001) 41–46, https://doi.org/10.1016/S0304-8853(00)01226-9.
[25] N.R. Jana, L. Gearheart, C.J. Murphy, Wet chemical synthesis of high aspect ratio cylindrical gold nanorods, J. Phys. Chem. B 105 (2001) 4065–4067, https://doi.org/10.1021/jp0107964.
[26] Y. Ni, X. Ge, Z. Zhang, Q. Ye, Fabrication and characterization of the plate-shaped γ-Fe_2O_3 nanocrystals, Chem. Mater. 14 (2002) 1048–1052, https://doi.org/10.1021/cm010446u.
[27] N. Hanžić, T. Jurkin, A. Maksimović, M. Gotić, The synthesis of gold nanoparticles by a citrate-radiolytical method, Radiat, Phys. Chem. 106 (2015) 77–82, https://doi.org/10.1016/J.RADPHYSCHEM.2014.07.006.
[28] T. Jurkin, M. Gulis, G. Dražić, M. Gotić, Synthesis of gold nanoparticles under highly oxidizing conditions, Gold Bull. 49 (2016) 21–33, https://doi.org/10.1007/s13404-016-0179-3.
[29] T.I. Sutherland, C.J. Sparks, J.M. Joseph, Z. Wang, G. Whitaker, T.K. Sham, J.C. Wren, Effect of ferrous ion concentration on the kinetics of radiation-induced iron-oxide nanoparticle formation and growth, Phys. Chem. Chem. Phys. 19 (2017) 695–708, https://doi.org/10.1039/C6CP05456K.
[30] E. Gachard, H. Remita, J. Khatouri, B. Keita, L. Nadjo, J. Belloni, Radiation-induced and chemical formation of gold clusters, New J. Chem. 22 (1998) 1257–1265, https://doi.org/10.1039/a804445g.
[31] J. Du, H. Liu, Preparation of superparamagnetic γ-Fe_2O_3 nanoparticles in nonaqueous medium by γ-irradiation, J. Magn. Magn Mater. 302 (2006) 263–266, https://doi.org/10.1016/J.JMMM.2005.09.016.
[32] B.G. Ekoko, R. Zhou, L. Xin, K.K. Lobo, L. Ilinga, Effects of pH on the morphology of iron oxides synthesized under gamma-irradiation, J. Radioanal. Nucl. Chem. 270 (2006) 473–478, https://doi.org/10.1007/s10967-006-0374-4.
[33] P.A. Yakabuskie, J.M. Joseph, P. Keech, G.A. Botton, D. Guzonas, J.C. Wren, Iron oxyhydroxide colloid formation by gamma-radiolysis, Phys. Chem. Chem. Phys. 13 (2011) 7198, https://doi.org/10.1039/c1cp20084d.
[34] A.H. Cuttler, V. Man, T.E. Cranshaw, G. Longworth, A Mössbauer study of green rust precipitates: I. Preparations from sulphate solutions, Clay Miner. 25 (1990) 289–301, https://doi.org/10.1180/claymin.1990.025.3.05.
[35] F. Trolard, J.-M.R. Génin, M. Abdelmoula, G. Bourrié, B. Humbert, A. Herbillon, Identification of a green rust mineral in a reductomorphic soil by Mossbauer and Raman spectroscopies, Geochim. Cosmochim. Acta. 61 (1997) 1107–1111, https://doi.org/10.1016/S0016-7037(96)00381-X.
[36] A. Zegeye, L. Huguet, M. Abdelmoula, C. Carteret, M. Mullet, F. Jorand, Biogenic hydroxysulfate green rust, a potential electron acceptor for SRB activity, Geochim. Cosmochim. Acta. 71 (2007) 5450–5462, https://doi.org/10.1016/J.GCA.2007.08.025.
[37] A. Géhin, C. Ruby, M. Abdelmoula, O. Benali, J. Ghanbaja, P. Refait, J.-M.R. Génin, Synthesis of Fe(II-III) hydroxysulphate green rust by coprecipitation, Solid State Sci. 4 (2002) 61–66, https://doi.org/10.1016/S1293-2558(01)01219-5.
[38] A. Sumoondur, S. Shaw, I. Ahmed, L.G. Benning, Green rust as a precursor for magnetite: an in situ synchrotron based study, Mineral. Mag. 72 (2008) 201–204, https://doi.org/10.1180/minmag.2008.072.1.201.
[39] C. Ruby, R. Aïssa, A. Géhin, J. Cortot, M. Abdelmoula, J.-M. Génin, Green rusts synthesis by coprecipitation of FeII–FeIII ions and mass-balance diagram, Compt. Rendus Geosci. 338 (2006) 420–432, https://doi.org/10.1016/J.CRTE.2006.04.008.
[40] G. Powis, M. Seewald, M. Hoke, Inhibition of growth factor binding and intracellular Ca^{2+} signalling by dextran sulfates of different sizes and degrees of sulfation, Cancer Chemother. Pharmacol. 30 (1992) 483–486, https://doi.org/10.1007/BF00685602.
[41] R. Yamagishi, M. Niwa, N. Sakuragawa, Thrombin inhibitory activity of heparin cofactor II depends on the molecular weight and sulfate amount of dextran sulfate, Thromb. Res. 44 (1986) 347–354, https://doi.org/10.1016/0049-3848(86)90009-5.
[42] Y. Chen, V.J. Mohanraj, J.E. Parkin, Chitosan-dextran sulfate nanoparticles for delivery of an anti-angiogenesis peptide, Lett. Pept. Sci. 10 (2003) 621–629, https://doi.org/10.1007/BF02442596.
[43] A. Fernandez-Martinez, V. Timon, G. Roman-Ross, G.J. Cuello, J.E. Daniels, C. Ayora, The structure of schwertmannite, a nanocrystalline iron oxyhydroxysulfate, Am. Mineral. 95 (2010) 1312–1322, https://doi.org/10.2138/am.2010.3446.
[44] J.M. Bigham, U. Schwertmann, L. Carlson, E. Murad, A poorly crystallized oxyhydroxysulfate of iron formed by bacterial oxidation of Fe(II) in acid mine waters, Geochim. Cosmochim. Acta. 54 (1990) 2743–2758, https://doi.org/10.1016/0016-7037(90)90009-A.
[45] R. Yuvakkumar, V. Elango, V. Rajendran, N. Kannan, Preparation and characterization of zero valent iron nanoparticles, Dig. J. Nanomater. Biostruct. 6 (2011) 1771–1776.
[46] H.C.B. Hansen, Composition, stabilization, and light absorption of Fe(II)Fe(III) hydroxy-carbonate ('green rust'), Clay Miner. 24 (1989) 663–669, https://

doi.org/10.1180/claymin.1989.024.4.08.
[47] D.J. Vaughan, M.S. Ridout, Mössbauer studies of some sulphide minerals, J. Inorg. Nucl. Chem. 33 (1971) 741–746, https://doi.org/10.1016/0022-1902(71)80472-4.
[48] K.A. Malini, M.R. Anantharaman, A. Gupta, Low temperature Mössbauer studies on magnetic nanocomposites, Bull. Mater. Sci. 27 (2004) 361–366, https://doi.org/10.1007/BF02704773.
[49] M. Usman, J.M. Byrne, A. Chaudhary, S. Orsetti, K. Hanna, C. Ruby, A. Kappler, S.B. Haderlein, Magnetite and green rust: synthesis, properties, and environmental applications of mixed-valent iron minerals, Chem. Rev. 118 (2018) 3251–3304, https://doi.org/10.1021/acs.chemrev.7b00224.
[50] V. Čuba, R. Silber, V. Múčka, M. Pospíšil, S. Neufuss, J. Bárta, A. Vokál, Radiolytic formation of ferrous and ferric ions in carbon steel – deaerated water system, Radiat. Phys. Chem. 80 (2011) 440–445, https://doi.org/10.1016/j.radphyschem.2010.09.012.
[51] J. Vandenborre, F. Crumière, G. Blain, R. Essehli, B. Humbert, M. Fattahi, Alpha localized radiolysis and corrosion mechanisms at the iron/water interface: role of molecular species, J. Nucl. Mater. 433 (2013) 124–131, https://doi.org/10.1016/j.jnucmat.2012.09.034.
[52] S.C. Reiff, J.A. LaVerne, Radiation-induced chemical changes to iron oxides, J. Phys. Chem. B 119 (2015) 7358–7365, https://doi.org/10.1021/jp510943j.
[53] J. Vandenborre, F. Crumière, G. Blain, R. Essehli, B. Humbert, M. Fattahi, Alpha localized radiolysis and corrosion mechanisms at the iron/water interface: role of molecular species, J. Nucl. Mater. 433 (2013) 124–131, https://doi.org/10.1016/j.jnucmat.2012.09.034.
[54] W.R. Martin, Chemical processes in estuarine sediments, in: Encyclopedia of Ocean Sciences, Elsevier, 2009, pp. 539–550, https://doi.org/10.1016/B978-012374473-9.00651-2.

Supplementary materials

The impact of dextran sulfate on the radiolytic synthesis of magnetic iron oxide nanoparticles

Ivan Marić[1], Goran Štefanić[2,3], Marijan Gotić[2,3,*],Tanja Jurkin[1,*]

[1]*Radiation Chemistry and Dosimetry Laboratory, Division of Materials Chemistry, Ruđer Bošković Institute, Bijenička 54, 10 000 Zagreb, Croatia*

[2]*Laboratory for Molecular Physics and Synthesis of New Materials, Division of Materials Physics, Ruđer Bošković Institute, Bijenička 54, 10 000 Zagreb, Croatia*

[3]*Center of Excellence for Advanced Materials and Sensing Devices, Research Unit New Functional Materials, Ruđer Bošković Institute, Bijenička 54, 10 000 Zagreb, Croatia*

[*]Corresponding authors: Tanja Jurkin, Ruđer Bošković Institute, Bijenička 54, 10000 Zagreb, Croatia, Phone: +385 1 4571 255, *E-mail address*: tjurkin@irb.hr

and

Marijan Gotić, Ruđer Bošković Institute, Bijenička 54, 10000 Zagreb, Croatia, Phone: +385 1 4561 123, *E-mail address*: gotic@irb.hr

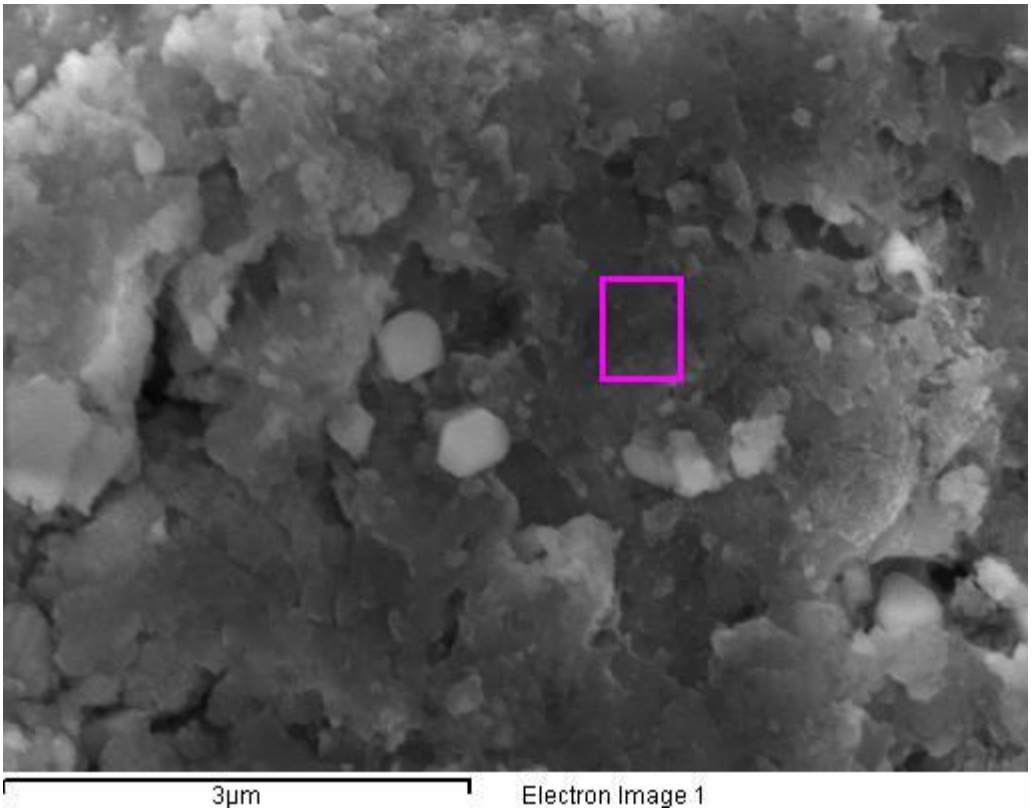

Element	weight%	mol %
C K	7.51	13.92
O K	32.87	45.75
Na K	21.53	20.85
P K	0.75	0.54
S K	11.23	7.80
Cl K	3.21	2.02
Fe K	22.91	9.13
Totals	100.00	

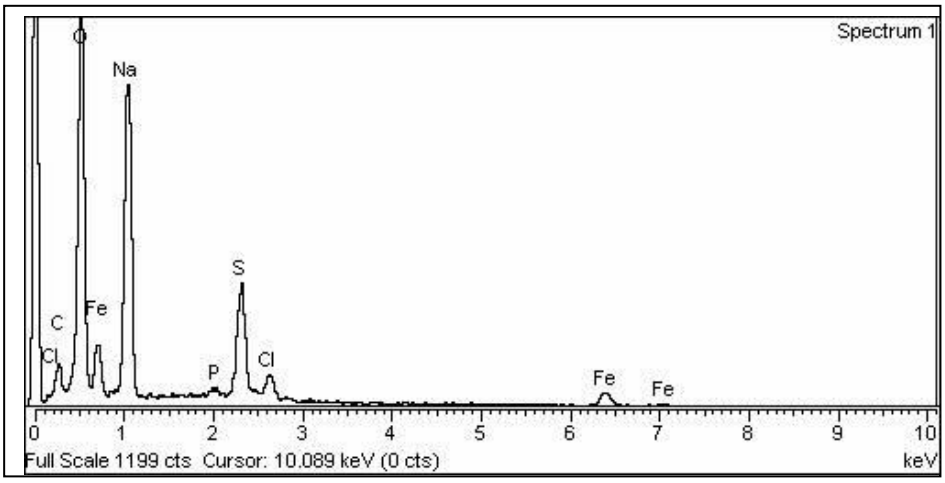

Fig. S1 Scanning Electron Microscopy (SEM) image and corresponding Energy Dispersive X-ray Spectroscopy (EDS) results (tabular and graphical presentations) of the sample that was not irradiated nor washed. (0 kGy, unwashed). The analysis was performed on the rectangular area bordered by purple color. The amount of carbon (C) in the sample is estimated to 13.92 mol % (the source of carbon is dextran polymer), however, this value is not reliable, because the powder sample is stick on the graphite tape that is also source of carbon. The high concentration of sodium (Na) is due to the added NaOH and dextran sulfate sodium salt (polymer). Besides, the relative very high concentration of sulfur and relatively high oxygen/iron molar ratio of 5.0 (45.75/9.13) is due to the sulfate groups in dextran sulfate polymer. In addition to sulfate groups, the possible source of oxygen are ether oxygen and hydroxyl oxygen in dextran sulfate polymer. The source of chloride (Cl) is iron salt ($FeCl_3$), whereas the phosphorus (P) is due to the phosphate buffer present in the dextran sulfate polymer.

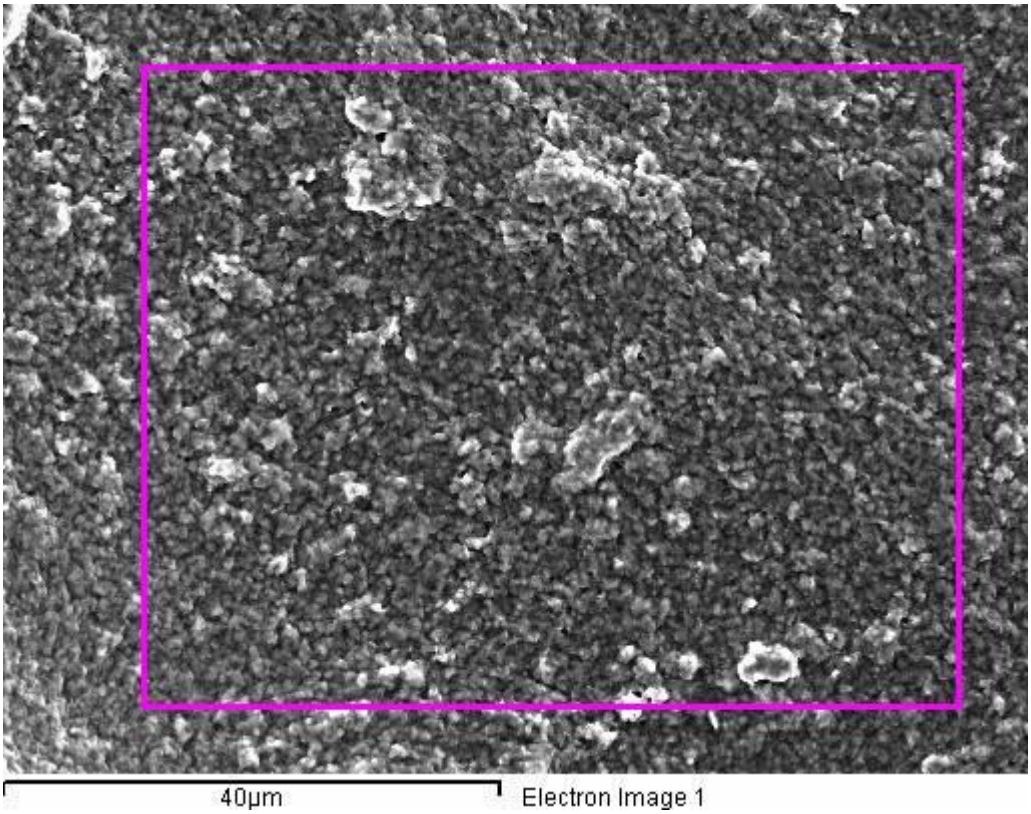

Element	weight%	mol%
C K	23.00	33.72
O K	48.80	53.70
Na K	4.22	3.23
P K	0.60	0.34
S K	5.79	3.18
Cl K	1.56	0.77
Fe K	16.04	5.06
Totals	100.00	

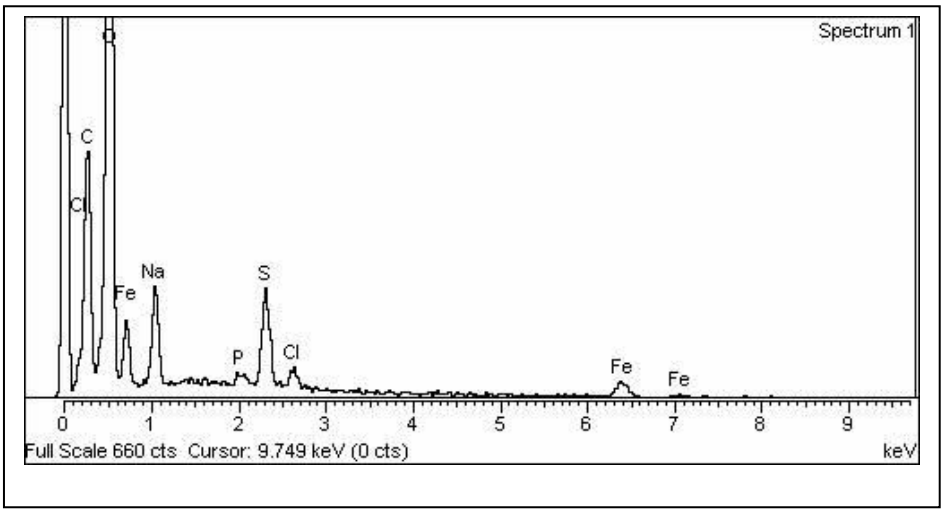

Fig. S2 SEM and EDS results (tabular and graphical presentations) of sample S-130G (130 kGy, isolated by admixing glycerol). The analysis was performed on the rectangular area bordered by purple colour. The large amount of carbon (C) in the sample is not reliable due to the graphite tape used as support, however much higher concentration of carbon in this sample can be explained by the fact that glycerol was admixed during the sample isolation.

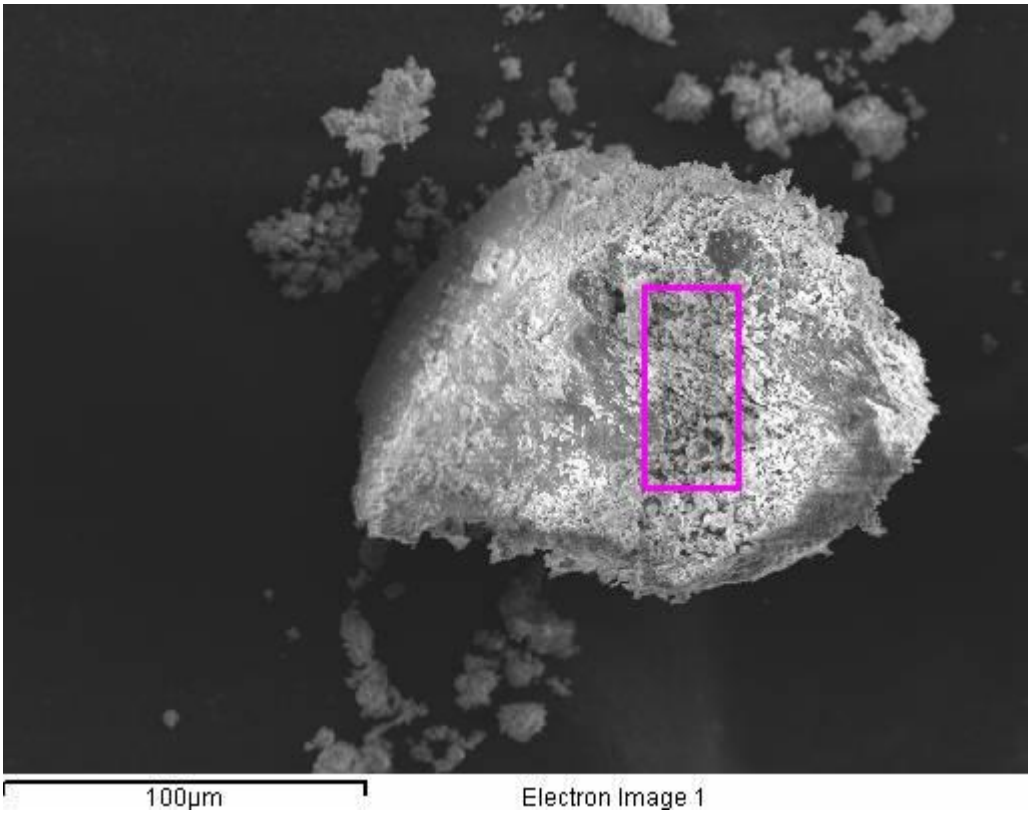

Element	weight%	mol %
C K	10.12	17.83
O K	45.71	60.46
Na K	4.70	4.33
P K	1.11	0.76
S K	7.46	4.92
Fe K	30.90	11.71
Totals	100.00	

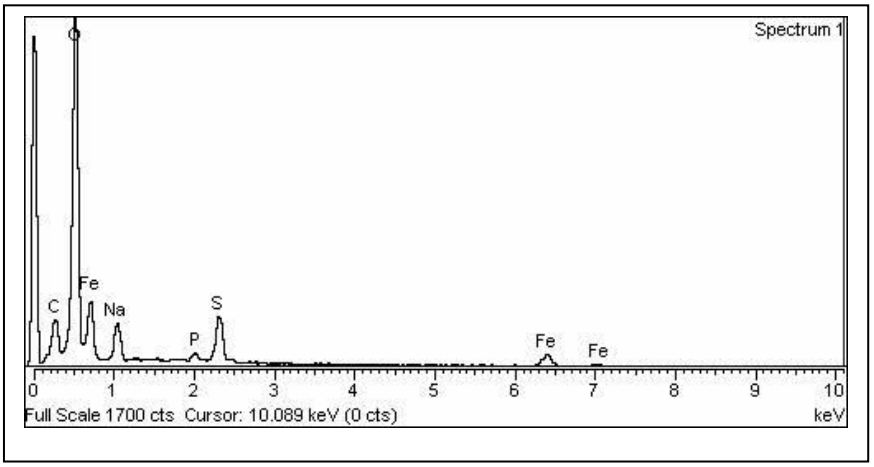

Fig. S3 SEM and EDS results (tabular and graphical presentations) of sample S-130E (130 kGy, sample was isolated by centrifugation and rinsed with ethanol). The analysis was performed on the rectangular area bordered by purple colour. The oxygen/iron molar ratio is 5.2, which is very high. The high O/Fe molar ratio is due to the low solubility of sulfate in ethanol. Sulfate groups that are part of dextran polymer (additional oxygen atoms) precipitate with ferrous - Fe(II) and ferric - Fe(III) ions thus increasing the relative concentration of sulfur and oxygen. Also, the samples isolated by rinsing with ethanol were relatively much lighter (more light elements such as sulfur, oxygen and carbon) in comparison with the samples isolated by washing with water (more iron).

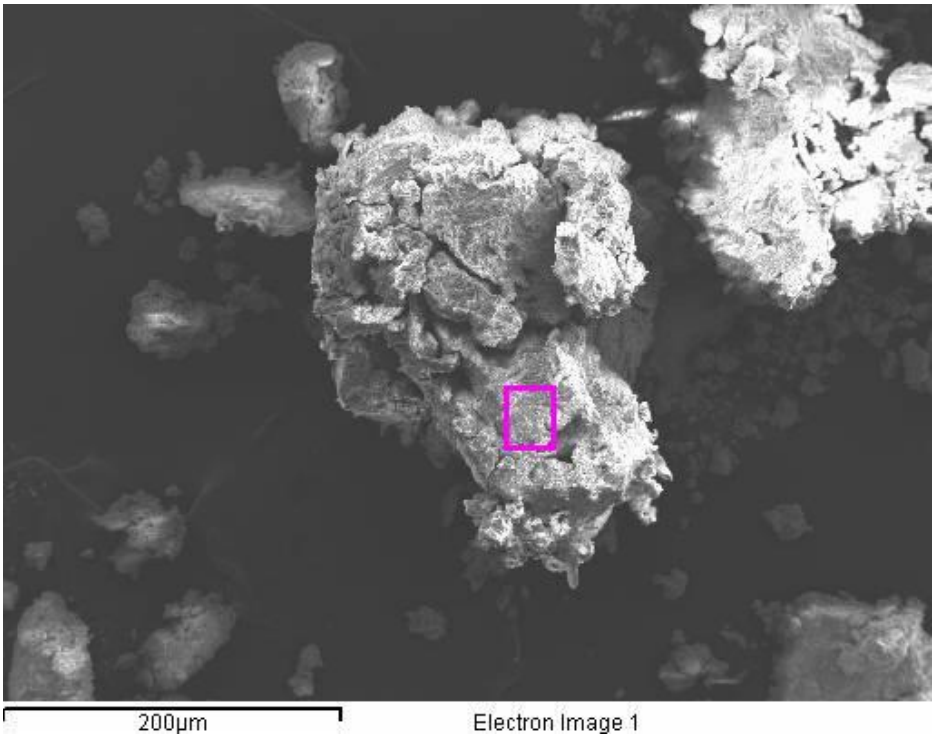

Element	Weight%	Atomic%
C K	4.87	10.47
O K	37.95	61.23
Na K	0.55	0.61
P K	0.66	0.55
S K	3.68	2.96
Fe L	52.30	24.18
Totals	100.00	

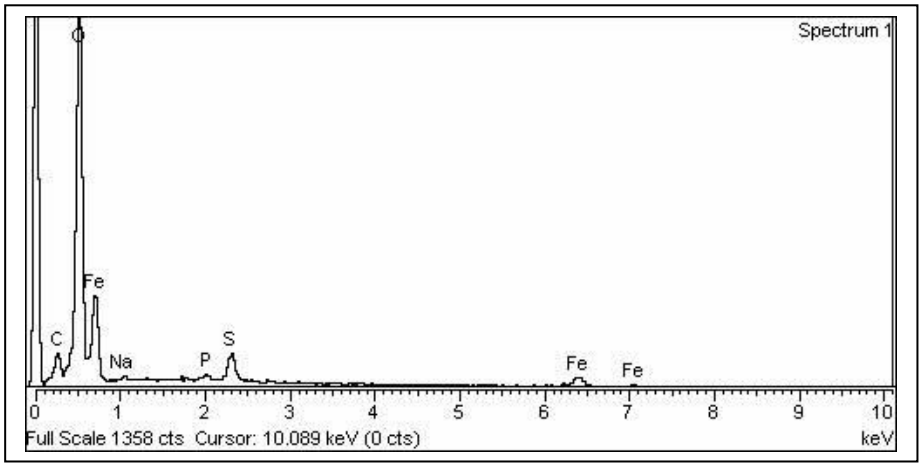

Fig. S4 SEM and EDS results (tabular and graphical presentations) of sample S-130W (130 kGy, sample was isolated by centrifugation and washed with water). The analysis was performed on the rectangular area bordered by purple colour. The oxygen/iron molar ratio is 2.5, which is much lower than in ethanol rinsed sample 130E (relatively much more iron). The content of sulfur is 2.96 mol %, which is almost 1 mol % less than in ethanol rinsing sample 130E. Since sulfates are more soluble in water, less sulfur is found in the precipitate. Due to these reasons ethanol rinsed samples have much higher oxygen/iron molar ratio (5.2 in sample S-130E) in comparison to the water washed samples (oxygen/iron molar ratio is 2.5 in sample S-130W).

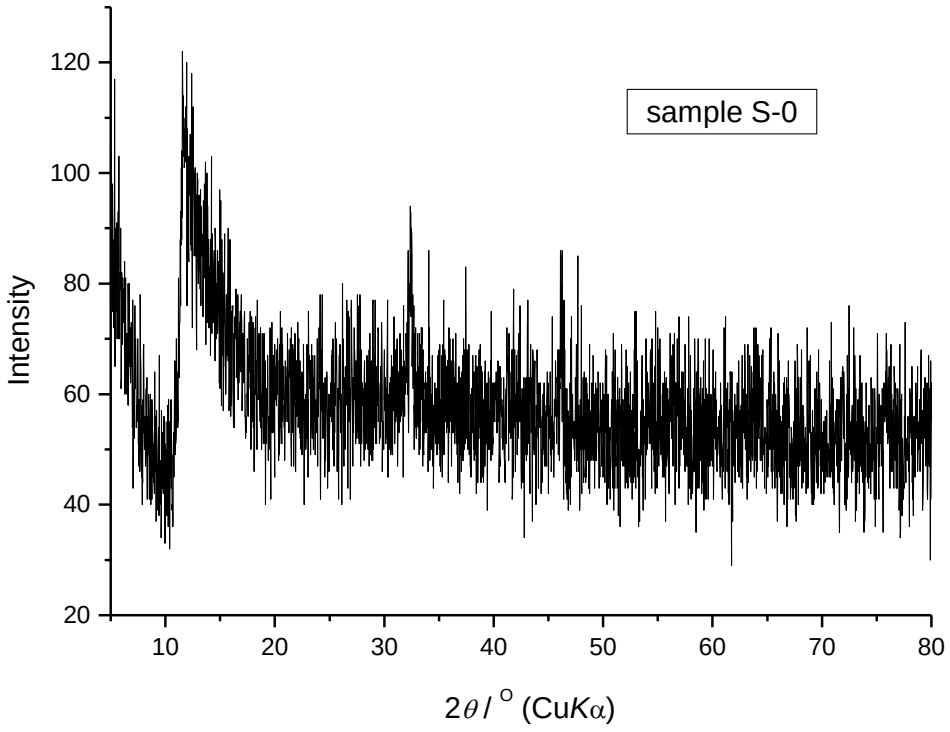

Fig. S5 The XRD patterns of isolated powder Fe(III) precursor that was not irradiated nor washed (sample S-0). The sample is of red colour. We did not manage to attribute these XRD patterns to any of iron oxide phases and due to this reason we denoted this sample as "$Fe(OH)_3$".